Journal of Proteomics 322 (2026) 105536

Contents lists available at ScienceDirect

Journal of Proteomics

journal homepage: www.elsevier.com/locate/jprot

Anisomelic acid promotes proteasomal degradation of HPV16 E6 via E3 ligase recruitment: A mass spectrometry-based interactome study

Michael Santos Silva [a,b,*], Leila S. Coelho-Rato [a,b], Navid Delshad [a,b], Tatiana Tarkhova [a,b], Joakim Edman [a,b,c], Preethy Paul [a,b], Annika Meinander [a,d], John E. Eriksson [a,b,e,*]

[a] Faculty of Science and Engineering, Cell Biology, Åbo Akademi University, 20520 Turku, Finland
[b] Turku Bioscience Centre, University of Turku and Åbo Akademi University, 20520 Turku, Finland
[c] School of Medicine, Medical Sciences and Nutrition, Aberdeen University, Aberdeen, UK.
[d] InFLAMES Research Flagship Center, Åbo Akademi University, 20520 Turku, Finland
[e] Euro-Bioimaging, ERIC, 20520 Turku, Finland

ARTICLE INFO

Keywords:
Anisomelic acid
Human papilloma virus
E6
Proteasomal degradation
E3 ligases
Mass spectrometry

ABSTRACT

Human papillomavirus (HPV) is a major driver of cervical and other epithelial cancers, with the viral oncoprotein E6 playing a central role in tumorigenesis by promoting degradation of the tumor suppressor p53. While prophylactic vaccines prevent infection, there remains a critical need for therapeutic strategies that eliminate established HPV-positive cells. Here, we identify anisomelic acid (AA), a natural diterpenoid, as a novel pharmacological principle that selectively induces the degradation of HPV16 E6. Using cellular thermal shift assay, we demonstrate that AA directly interacts with E6, likely triggering a conformational change that promotes its ubiquitination. Proteomic analysis of the E6 interactome in AA-treated cells revealed consistent enrichment of E3 ubiquitin ligases, including E6AP, UBR4, CDC20, and TRIP12, as well as proteasomal subunits. To our knowledge, this represents the first comprehensive proteomics framework of the HPV16 E6 interactome under small-molecule treatment conditions. These findings support a model in which AA facilitates proteasome-mediated elimination of E6, and the dataset itself provides a timely and valuable resource for HPV biology and therapeutic development.

1. Introduction

Human papillomavirus (HPV) is a small DNA virus with the ability to infect mucosal and cutaneous epithelia. “Low-risk” HPVs are associated with the development of warts, whereas “high-risk” HPVs are the primary cause of certain types of cancers, including cervical cancer [1,2]. In 2022, cervical cancer was reported to be the fourth leading cause of cancer incidence and mortality among women globally [3]. Furthermore, reports estimated that over 600,000 women and 70,000 men are diagnosed with HPV-caused cancers each year. These numbers comprise numerous other types of malignancies linked to HPV, including anal, vaginal, penile, and head and neck cancers [4,5]. While HPV is often associated with women, a recent study reveals a concerning trend: nearly one-third of men over the age of 15 are infected with at least one type of genital HPV. Additionally, one in five of these men carry high-risk HPV types associated with cancer development [6].

HPV-mediated carcinogenesis is driven by two viral oncoproteins, E6 and E7. These exploit crucial molecular mechanisms which facilitate transformation [7]. The E6 oncoprotein is predominantly known for its ability to bind and promote the proteasomal degradation of the tumor suppressor p53. In non-cancerous cells, the activation of p53 is essential for cell stress responses, such as DNA damage, where it either arrests the cell cycle to allow for DNA repair or, in instances of irreparable damage, triggers apoptosis [8]. However, in HPV-positive cancer cell lines, E6 interacts with the E6-associated protein (E6AP/UBE3A) and compromises these crucial processes via ubiquitination and subsequent targeting of p53 for proteasomal degradation, which contributes to genomic instability [9,10]. In parallel, E7 affects retinoblastoma protein (pRb), another well-established tumor suppressor [11]. By interacting with and promoting the degradation of pRb, the regulatory mechanisms that modulate the cell cycle are disrupted, leading to uncontrolled cellular proliferation [12]. The combined actions of these oncoproteins establish a favorable environment that promotes tumorigenesis, making them valuable targets for therapeutic strategies against HPV-mediated

* Corresponding authors at: Faculty of Science and Engineering, Cell Biology, Åbo Akademi University, 20520 Turku, Finland.
E-mail addresses: michael.santossilva@abo.fi (M. Santos Silva), john.eriksson@abo.fi (J.E. Eriksson).

https://doi.org/10.1016/j.jprot.2025.105536
Received 10 July 2025; Received in revised form 27 August 2025; Accepted 15 September 2025
Available online 16 September 2025

cancers.

Despite the availability of vaccines designed to target several HPV types, this strategy is preventive and fails to be effective in individuals already infected with the virus. Therefore, an approach that selectively targets the E6 and E7 oncoproteins could potentially provide a more effective and less toxic alternative to current therapies, as it would specifically affect HPV-positive cells. Although E6 has been studied for decades, remarkably little is known about its interactome under pharmacological perturbation. Based on this knowledge gap, our laboratory previously investigated the natural compound anisomelic acid (AA), isolated from *Anisomeles malabarica*, and demonstrated that AA downregulates E6 and E7, stabilizes their targets p53 and p21, and induces cell-cycle arrest and apoptosis. These findings highlighted AA's therapeutic promise, but the molecular mechanism and interactome-level changes underlying E6 downregulation remained undefined. Furthermore, our research indicates minimal cytotoxic effects of AA on uninfected cells, underscoring its potential as a safe alternative to conventional treatment strategies. We also demonstrated that treatment with AA leads to a significant decrease in endogenous E6 protein levels in HPV16-positive cervical cancer cells. This effect, however, is inhibited in the presence of the proteasomal inhibitor MG132, suggesting that AA promotes E6 degradation through a proteasome-dependent mechanism [13].

Despite the clear role of AA in E6 downregulation, the molecular mechanism underlying this phenomenon remains unknown. Given these prior findings, we hypothesized that AA directly interacts with E6 and promotes its degradation via the proteasomal pathway. Thus, the objective of this study was to investigate the molecular mechanism by which AA induces degradation of E6 by establishing a model system for an unbiased mass spectrometry (MS)-based proteomics screen aimed at identifying key regulators of E6 stability.

We first show that E6 is ubiquitinated and downregulated via the proteasomal degradation pathway and provide evidence that AA directly binds E6. Then, using normal oral keratinocytes (NOKs) cell model stably expressing HPV16 FLAG-tag E6, we mapped the E6 interactome. This unbiased approach provided a thorough way to identify potential E3 ligases that may potentially target E6 for degradation. Furthermore, our analysis also shows that AA treatment leads to enrichment of biological processes like response to heat, chaperone-mediated protein folding, proteasomal and ubiquitin-related processes.

By elucidating the molecular basis of AA-mediated E6 degradation and identifying novel interactors involved in this process, this study offers valuable insights that could help the development of AA-like small molecules for targeted therapies for HPV-positive cancers.

2. Experimental procedures

2.1. Cell Culture, treatments and transfections

SiHa cells (HTB-35, ATCC) were cultured in Dulbecco's Modified Eagle Medium (DMEM; D6171, Sigma), supplemented with 4500 mg/L glucose, 10 % fetal bovine serum (FBS; S1810, Biowest), 100 U/mL penicillin and 100 μg/mL streptomycin (P0781, Sigma), 2 mM L-glutamine (X0550, Biowest).

To study the effects of AA on E6 proteins levels, the cells were transfected with N-CMV-HA-FLIP-16E6 (kind gift from Prof. Karl Munger), or pCMV-Neo-Bam (16440, addgene). Cells were transfected using electroporation. 3×10^6 cells were resuspended in 800 μL Opti-MEM (31–985-062, Gibco) and mixed with 10 μg of plasmid in 0.4 cm Gene Pulser/MicroPulser Electroporation Cuvettes (1652081, Bio-Rad). Electroporation was performed with a Gene Pulser II electroporator (Bio-Rad) using a single electric pulse (220 V, 975 μF). Cells were then transferred to supplemented DMEM, counted, and 0.3×10^6 cells were plated and cultured for 24 h. 24 h post-transfection control samples were treated with DMSO, and the other samples were treated with 20 μM of MG132 (S2619, Selleck chemicals) for 2 h, washed with PBS, and then treated with 40 μM of anisomelic acid for 24 h.

Normal oral keratinocytes stably expressing HPV16 E6 and E7 oncogenes (NOK16) and its parental negative control (pWPI) were kindly gifted by Dr. Martina Niebler (DKFZ, Germany) and were grown following the reported protocol [14]. Briefly, to ensure stable expression of both oncoproteins, the construct is under the control of a EF1α promoter and a self-cleaving P2A sequence was added between the E6 and E7 ORFs [14]. To test the usability of the cell line in our study, we treated them with 10, 20 or 40 μM of AA for 24 h and used them for imaging and western blot. For co-immunoprecipitation experiments, cells were treated with 20 μM AA, 5 μM MG132, or 5 μM Bortezomib (S1013, Selleck Chemicals). MG132 and Bortezomib samples were washed 1 h after treatment but only collected at the 24-h mark, together with AA treated samples. Control samples were treated with DMSO.

2.2. SDS-PAGE and western blot

Cells were collected, lysed and heated for 5 min at 98 °C in 1× laemmli sample buffer (#1610737, Bio-Rad) with 2.5 % β-mercaptoethanol. The lysates were loaded and separated on a 4–20 % Mini-PROTEAN® TGX (4561093 and 4561096, Bio-Rad) in 1× Tris/Glycine Buffer (#1610771, Bio-Rad) with 0.1 % SDS for 40 min at 200 V. Proteins were then transferred to methanol-activated polyvinylidene difluoride (PVDF) membranes (10600023, Amersham) using a wet transfer system filled with 1× Tris/Glycine Buffer with 20 % methanol, for 1 h at 400 mA. Membranes were blocked with 5 % milk in TBS 0.3 % Tween20, for 1 h, washed, and incubated with primary antibody overnight. Primary antibodies were diluted 1:1000 in TBS or PBS 0.3 % Tween20 3 % BSA 0.02 % sodium azide. Membranes were washed for 20 min with TBS or PBS 0.3 % Tween20, followed by 1 h incubation at room temperature with secondary antibody, which was diluted 1:10000 in TBS or PBS 0.3 % Tween20 5 % milk. Antibody detection was done using chemiluminescence (2 parts of Amersham RPN2109 to 1 part RPN2236) and detected with an iBright Imaging System (CL1000, Thermo). The following list of primary and secondary antibodies were used: HA (3724S, CST), HSC70 (ADI-SPA-815, Enzo), FLAG (F1804, Sigma), PARP (9542, CST), Caspase-3 (9661, CST), β-actin (5125S, CST), E6AP (7526S, CST). anti-Rabbit (W401B, Promega), anti-mouse (W4021, Promega), anti-rat (NA935, GE).

2.3. Tandem ubiquitin binding entities (TUBEs) pulldown

SiHa cells were transfected by electroporation and treated with MG132 and AA 24 h post-transfection, as previously explained. Cells were then trypsinized and lysed for 10 min, on ice in a lysis buffer containing: 20 mM disodium phosphate, 20 mM monosodium phosphate, 1 % NP-40, 2 mM EDTA, 1 % SDS, 1 mM DTT, 5 mM N-ethylmaleimide, 5 mM chloroacetamide and 1× Protease and phosphatase inhibitor (a32961, ThermoFisher Scientific). Samples were diluted to a final concentration of 0.1 % SDS and centrifuged at 12000 rpm for 10 min, at 4 °C. The supernatant was collected and 20 μL of 50 % slurry glutathione beads +6 μL of TUBE were added to the samples. The samples were kept for 2 h at 4 °C rotating and washed four times with PBS 0.1 % Tween20. The beads were collected and boiled in 50 μL laemmli. Samples were analyzed with SDS-PAGE and western blot.

2.4. Co-immunoprecipitation

Co-IP was performed in NOK cells for mass spectrometry analysis. Four biological replicates of each treatment condition were used (untreated, AA, AAMG). After treatments, cells were washed with PBS, collected in 500 μL lysis buffer (50 mM Tris-HCl pH 7.5, 150 mM NaCl, 0.5 % IGEPAL CA-630, 1× Protease and phosphatase inhibitor), lysed on a rotator for one hour at 4 °C. Then, samples were centrifuged at 13000 *g* for 10 min at 4 °C. 10 % of each supernatant were saved as input control, and the remaining used for co-IP. 25 μL of Anti-FLAG® M2 Magnetic

Beads (M8823, Sigma) were washed three times with PBS and then added to the samples used for IP. Samples were incubated on a rotator overnight at 4 °C and then washed three times with PBS. The final co-immunoprecipitates were either boiled in 50 µL Laemmli for western blot or prepared for mass spectrometry experiment.

2.5. CETSA

NOK16 cells were seeded on 15 cm plates at 70 % confluency in Experimental Media overnight (72.5 % F-12, 22.5 % DMEM, 5 % FBS, 5 µg/mL Insulin, 10 ng/mL Epidermal growth factor, 8.4 ng/mL Cholera toxin, 24 µg/mL Adenine, 0.4 µg/mL Hydrocortisone and Pen/Strep). The next day, cells were treated with DMSO or 20 µM AA for 1 h and then washed with PBS before trypsinization. Trypsinized cells were centrifuged at 300 *g* for three minutes, washed and resuspended in 1 mL of PBS. 100 µL cell aliquots were heat treated with different temperatures (43, 47, 50, 53, 57 and 60 °C) for three minutes using a thermal cycler, followed by three minutes at room temperature. The samples were snap-frozen in dry ice, and stored at −80 °C. For western blot analysis, cells were lysed by three freeze-thaw cycles in dry ice and vortex in between. Samples were centrifuged at 20000 *g* for 20 min at 4 °C and supernatants mixed and boiled in 2× Laemmli buffer.

2.6. Mass spectrometry

Co-IP samples were washed three times with lysis buffer (50 mM Tris-HCl pH 7.5, 150 mM NaCl, 0.5 % IGEPAL CA-630, 1× Protease and phosphatase inhibitor), three times with ice cold PBS and three times with MilliQ water. Next, samples were digested using an on-bead digestion approach. Beads were digested with 5 µg/mL trypsin in 6 volumes of 2 M urea, 25 mM ABC pH 7.5 and incubated on a thermomixer at 800 rpm, for 30 min at 27 °C. Supernatants were collected to separate tubes, and the beads washed twice with 2.5 volumes of 2 M urea, 25 mM ABC pH 7.5 with 1 mM DTT. Supernatants were pooled together and digested overnight at room temperature. The next day, 20 µL of 5 mg/mL IAA was added for 30 min, in the dark. Samples were acidified with trifluoroacetic acid (TFA) and desalted using a Sep-Pak C18 96-well plate (40 mg, 186003966, Waters) according to manufacturer instructions. Samples were then dried using a speed-vac centrifuge and stored at −80 °C. Samples were dissolved in 0.1 % formic acid, prior to loading. 400 ng of each sample was used for LC-MS/MS analysis.

Peptides were analyzed using an EASY-nLC 12000 HPLC system (Thermo Fisher Scientific) linked to an Orbitrap Fusion Lumos mass spectrometer (Thermo Fisher Scientific), which featured a nano-electrospray ionization source. Samples were loaded onto a trapping column (100 µm internal diameter × 2 cm) and subsequently separated on an analytical column (75 µm internal diameter × 15 cm). Both columns were prepared in-house using ReproSil-Pur C18-AQ resin (3 µm, 120 Å; Dr. Maisch HPLC GmbH). The elution was done using a 60-min gradient (8–21 % solvent B over 28 min, 21–36 % B over 22 min, 36–100 % B over 5 min, followed by a final wash at 100 % B for 5 min), with solvent B being an acetonitrile/water mixture (80/20) containing 0.1 % formic acid, run at a constant flow of 300 nL/min. Full-scan MS spectra were obtained in the Orbitrap over an m/z range of 300–1750 at a resolution of 120,000. The automatic gain control (AGC) target was configured to 700,000, with a maximum injection duration of 50 ms. Precursor ions with charge $> +2$ and intensity >25,000 were selected for fragmentation within a cycle time of 2.5 s. These were then isolated in the quadrupole utilizing a 1.6 Da window and underwent fragmentation via higher-energy collisional dissociation (HCD) at a normalized collision energy of 27 %. MS/MS spectra were acquired in the Orbitrap at a resolution of 30,000, with an AGC target of 50,000 and a maximum injection time of 75 ms. Dynamic exclusion parameters were established at 35 s with a mass tolerance of 10 ppm.

The raw LC-MS/MS data were processed using MaxQuant (2.0.1.0) [15,16] or FragPipe software (version 21.1) alongside msFragger (version 4.0), IonQuant (version 1.10.12), Philosopher (version 5.1.0) and Python (3.9.13) [17–19].

For the MaxQuant search we used Uniprot HPV (UP000009251, 9 entries) and human proteome (UP000005640, 78120 entries), both downloaded on August 1st 2021, including contaminants from MaxQuant database. Group-specific parameters included methionine oxidation and acetylation (protein n-term) as a variable modification, carbamidomethylation as a fixed modification and trypsin digestion with a maximum of 2 missed cleavages allowed. Mass tolerance settings set for 20 ppm for first search and 4.5 ppm for main search. Label-free quantification was enabled, with a minimum ratio count of 2 and classic normalization type, considering unique+razor peptides for quantification. False discovery rate (FDR) was set to 1 %, and match between runs enabled to a 2-min match time window and an alignment time window of 20 min. Downstream analysis was done using Perseus (1.6.15.0) [20]. Contaminants, reverse sequences and only identified by site hits were removed and data was transformed and filtered for three values in at least one group. At least three replicates were used for analysis. Venn diagrams were generated from InteractiVenn [21] with the median average of replicates at different stages of the analytical pipeline. Data was imputed based on normal distribution (width 0.3, down shift 1.8, total matrix) and filtered for ANOVA significance (p-value <0.05). Z-scored data with Euclidean distance was used to generate the Hierarchical clustering heatmaps. Ontology analysis was performed with ShinyGo 0.80 [22] using a human background and focusing on the top 10 biological processes with a 0.05 FDR cutoff and minimum pathway size of 2. Hawaii plots were created in Perseus using Pearson correlation. Data that was not imputed was filtered using a ratio E6/pWPI >1.05.

For the FragPipe searches, the UniProt human protein database (UP000005640) was downloaded on September 5, 2023. This database contained a total of 40912 entries, with 50 % generated reverse decoys. The default LFQ-MBR workflow was used. The parameters were as follows: precursor and fragment mass tolerance of 20 ppm, trypsin digestion allowing a maximum of two missed cleavages, methionine oxidation selected as a variable modification and cysteine carbamidomethylation as a fixed modification; FDR was set to 1 % for both protein and peptide levels. Downstream analysis was performed with Perseus (following the same approach mentioned previously for MaxQuant data) and the output file reprint.int was used in CRAPome [23] for SAINT [24] analysis, using SAINT with user controls and default settings.

2.7. Imaging and image processing

Phase contrast images of NOK16 and NOKs pWPI were taken at 0 h and 24 h post-AA treatment using a Zeiss AxioVert microscope, with a 10× dry objective.

Raw .czi files were loaded into ZenLITE (version 3.1.101.05) and batch-exported as native 8-bit TIFF files without modifications. These TIFF files were subsequently imported into Ilastik (version 1.4.0. post1) [25] for pixel classification. In the classification workflow, feature selection was based on Sigma 1–6 parameters, including Gaussian smoothing, Laplacian of Gaussian, Gaussian gradient magnitude, difference of Gaussians, structure tensor eigenvalues, and Hessian of Gaussian eigenvalues. Images were classified into four categories: alive, dead, plate and borders. Manual pixel classification was performed using the brush tool (radius = 1) to mark distinguishing features. The generated probability maps were exported as multipage TIFF files, which were further processed in ImageJ FIJI (version 2.16.0) [26] using scripting to separate the multipage TIFFs into individual slices labelled as alive, dead, plate and borders. For cell quantification, CellProfiler (version 4.2.6) was used [27]. Metadata embedded in file names was extracted using the regular expression (?P < Slice>.{9})_(?P < Experiment>.{5}).

Prior to analysis, 10 nuclei classified as “alive” and 10 as “dead” were characterized for each condition using FIJI’s area measurement tool to

determine parameters for primary object classification. The following functions were applied to the imported probability map to differentiate between dead and alive cells: Identify primary objects (automatic thresholding, threshold smoothing 0.348, minimum radius 15 px^2, erosion ($r = 1$)), measure object size shape, measure object intensity. Eroded nuclei were superimposed on original images using function overlay objects for quality control (opacity 0.4). Overlay images were exported in 32-bit TIFF format for quality assurance. Data was exported in CSV format for downstream analysis. Initial data re-structuring was done using Microsoft Excel (Ver. 2406). Data filtering was subsequently performed to exclude nuclei with an area ≤ 100 px^2 based on previous nuclei characterization. On remaining data (−15 % filtered) the following characteristics were calculated: number of total nuclei, % alive, and %dead.

SPSS (Ver. 27.1) was used for statistical analysis. Variables included time (0H, 24H), treatment (DMSO, 10 AA, 20 AA, 40 AA), vector type (empty vector, E6/E7 plasmid), and biological repeats (Repeat 1, Repeat 2). The analysis was conducted using a General Linear Model with Tukey's post hoc tests. Further statistical analysis and data visualization were performed using GraphPad PRISM (version 9.0).

2.8. Artwork

Illustration in Fig. 3 was created in Adobe Illustrator. Graphical abstract was created in BioRender. Eriksson, J. (2025) https://BioRender.com/en34kmf

3. Results and discussion

3.1. Anisomelic acid leads to the ubiquitination and downregulation of exogenous HPV16 E6

To investigate the molecular mechanism underlying AA-mediated E6 degradation and to identify potential interacting partners, we first established a model suitable for mass spectrometry (MS)-based analysis. SiHa cells were transiently transfected with HPV16 E6-FLAG-HA. 24 h post-transfection, the cells were pretreated with 20 μM MG132 for two hours, followed by 24 h exposure to 40 μM AA. In line with the results from our previous report [13], we observed a decrease in E6 protein levels after AA treatment, while the presence of MG132 prevented its effects, reinforcing the hypothesis that AA-mediated E6 degradation is proteasome-dependent (Fig. 1A).

Since E6 is degraded by the proteasome, we hypothesized that E6 was ubiquitinated, a crucial post-translational modification to target proteins for degradation. To test this, we performed the same transfection and treatment procedures, but this time followed by an enrichment of ubiquitinated proteins using tandem ubiquitin binding entities (TUBEs) pulldown. Our results show that samples treated with AA have increased amounts of ubiquitinated E6 when compared to untreated samples. Furthermore, in samples treated with MG132, the accumulation of ubiquitinated E6 was even more pronounced in the presence of AA (Fig. 1B). These findings indicate that AA enhances the ubiquitination of E6, facilitating its degradation via the proteasomal pathway. E6 ubiquitination plays an important role for E6/E6AP-mediated p53 degradation, and can be modulated by cellular factors such as USP15 and p53 mutant R175H [28]. Others have shown that docosahexaenoic acid downregulates E6 and E7 protein levels by activating the ubiquitin–proteasome system through increased ROS production, which also caused increased ubiquitination of E6 after treatment [29]. However, the mechanism underlying this effect has not been investigated yet. In our case, although we have not checked ROS levels, we considered two possible mechanisms: one could be that AA activates an upstream regulator, such as an E3 ligase, leading to increased E6 ubiquitination; alternatively, AA could directly bind to E6, a conformational change that makes it more susceptible to ubiquitination by E3 ligases. Thus, to investigate whether AA could directly bind E6 we performed a cellular thermal shift assay (CETSA) [30] using NOKs stably expressing HPV16 FLAG-tag E6 (NOK16) [14]. CETSA is based on the principle that the thermal stability of a protein can change upon direct ligand binding, with bound proteins typically exhibiting increased resistance to heat-induced denaturation. So, we treated NOK16 with DMSO or 20 μM of AA and heated them at different temperatures. We found that, in the presence of AA, E6 exhibits increased thermal stability, as evidenced by more intense protein bands at 47 °C and 50 °C, when compared to DMSO controls (Fig. 2A). These results complement the observation found by an in silico approach, which reveals that AA weakly binds to the E6 binding pocket [31]. These findings, together with the previous in silico evidence, strongly suggest that AA directly interacts with E6. This interaction is likely to alter E6 conformation in a way that enhances its ubiquitination and subsequent degradation. Importantly, the persistent technical barrier of producing sufficient amounts of folded E6 protein makes CETSA a uniquely feasible and physiologically relevant approach in this context. CETSA has been successfully applied in many studies of similarly "difficult" proteins, with subsequent structural or genetic work

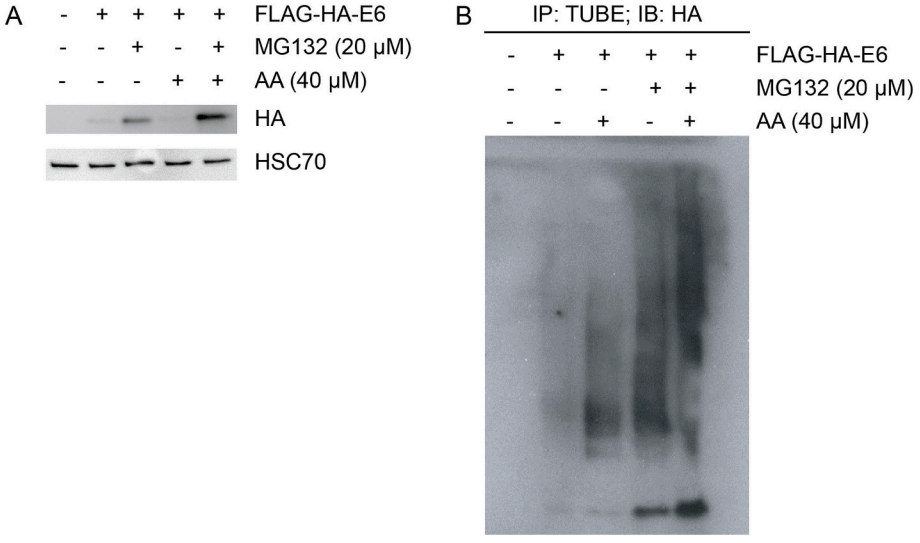

Fig. 1. AA induces proteasomal degradation of HPV16 E6. a) Western blot analysis of SiHa cells subjected to transfection with HPV16 E6-FLAG-HA and treated 24 h post-transfection with MG132 for 2 h and/or with AA for 24 h. HSC70 was used as the loading control. b) TUBE pulldown of transfected SiHa cells were treated with MG132 (2 h) and/or AA (24 h) for 24 h.

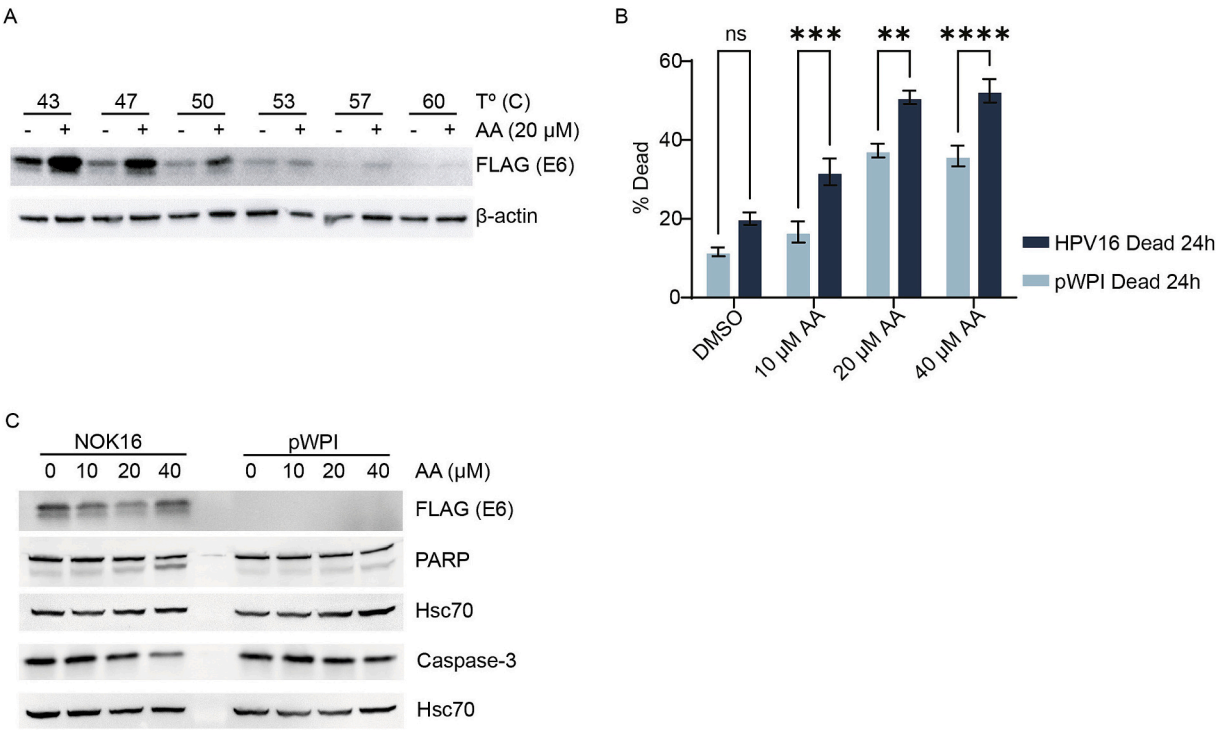

Fig. 2. AA leads to E6 downregulation and cell death in NOKs stably expressing HPV16 FLAG-tag E6. a) Western blot analysis of NOKs treated for 24 h with AA. HSC70 was utilized as loading control. b) Phase contrast images were analyzed using Ilastik, Fiji and cell profiler to plot the percentage of dead cells, which show an increased amount in AA-treated NOK16 samples. c) Western blot analysis of the CETSA assay. NOKs cells were trypsinized, collected and heated at varying temperatures, ranging from 43 to 60 °C, both in the presence and absence of AA.

validating its findings [30,32–35], further underscoring the robustness of our approach. Future research would benefit from other techniques to elucidate the binding affinity and kinetics of AA-E6, such as isothermal titration calorimetry or surface plasmon resonance, or methods to map AA binding sites, like x-ray crystallography or cryo-EM, would be beneficial, although they require purified protein, which has been proven challenging.

Finally, to further explore the degradation pathway and potentially identify the E3 ligase that targets E6 for ubiquitination, we employed mass spectrometry-based proteomics using NOKs stably expressing HPV16 FLAG-tag E6 and STREP-tag-E7. The stable expression of HPV16 FLAG-tag E6 not only minimizes the variance due to discrepancies in transfection efficiency across replicates but also eases the co-immunoprecipitation (co-IP) procedure and sample preparation, resulting in an overall more robust dataset. When these cells were generated, the expression of both E6 and E7 were tested with quantitative PCR, which showed E6 and E7 expression levels comparable to those found in HPV16-positive CaSki cells [14]. To ensure that this cell line was suitable for our study, we monitored the effects of the different concentrations of AA using imaging and western blot. We observed increased cell death in E6-expressing cells following AA treatment, compared to the negative control (pWPI) cells (Fig. 2B and S1A). Western blot analysis further confirmed that AA led to a marked decrease in E6 in NOK16 cells (Fig. 2C). Additionally, we observed PARP cleavage and decreased levels of caspase-3 in E6-expressing cells, which is consistent with increased apoptosis. These findings are in line with our previous observations and support the role of AA in promoting E6 degradation and consequent apoptosis of HPV-positive cells [13]. However in this cell line at 40 μM there are higher E6 protein levels which was not observed in SiHa cells. This could be because at higher concentrations, some compounds can trigger cellular stress responses, such as oxidative stress or the unfolded protein response, which may unintentionally increase E6 expression or block its degradation. For example, oxidative stress has been shown to enhance E6 levels in HPV-positive head and neck cancer cells, while ER stress can disrupt protein degradation pathways [36,37]. Therefore, the higher E6 levels at 40 μM concentration could result from stress-induced cellular mechanisms that enhance E6 expression or inhibit its degradation pathways. Therefore, a 20 μM dose was selected for subsequent studies employing a proteomics-based approach. Additionally, the PARP cleavage and reduction in caspase-3 levels observed at 40 μM may result from off-target effects that induce cellular stress, leading to apoptosis independent of E6 expression levels. For instance, ER stress has been shown to induce apoptosis through PARP cleavage, even when viral oncoproteins like E6 are elevated. Additionally, oxidative stress can lead to DNA damage and activation of apoptotic pathways, resulting in similar outcomes [38]. Since these are oral keratinocytes, inherent differences in cellular robustness and sensitivity may account for the observed changes. Nonetheless, these findings support the suitability of this NOK cell model for investigating the E6 interactome and the mechanism of action of AA at the selected 20 μM dose.

Next, to ensure that AA does not interfere with co-IP experiments, we performed a FLAG pulldown, and successfully detected E6AP, a well-established interactor of E6 [39], in samples across all treatments (Fig. S1B). This indicates that AA does not disrupt protein-protein interactions, further validating our experimental approach for mass spectrometry-based proteomics. Furthermore, other proteomics studies have been done using, for instance, N/Tert-1 cells [40] to study the HPV-associated proteome across different HPV types, or NOKs [14] for a combined transcriptomic and proteomics analysis of changes made by the viral oncogenes. However, no study has yet been done to address the changes in HPV E6 interactome under drug treatment conditions. Thus, our study provides the first unbiased evidence that a small-molecule compound can reshape the HPV16 E6 interactome in living cells. This represents a conceptual and technical advance, expanding beyond the well-characterized E6AP interaction and offering a dataset that will guide both mechanistic and translational research.

Collectively, our results suggest that AA promotes HPV16 E6

degradation through enhanced ubiquitination and proteasomal targeting, which is in line with previous reports on the effects of AA on endogenous levels of E6 [13]. Moreover, the fact that we could replicate the effects of AA seen in HPV-positive cervical cancer cells in transformed oral keratinocytes points to a generalized mechanism among HPV-positive cells and validates the use of NOKs to study the mechanism of action of AA. Crucially, we show for the first time that AA can directly bind E6, which supports the hypothesis that the binding of AA might increase E6's susceptibility to proteasomal degradation.

3.2. E6 interactome after AA treatment reveals enrichment of multiple proteasomal subunits and E3 ligases

To investigate the role of AA in E6 degradation, we next aimed to use NOK cells to find the E3 ligase involved in this mechanism. To achieve this, we performed co-IP of FLAG in different conditions ($n = 4$): NOK pWPI left untreated to be used as a negative control for the co-IP (pWPI), NOK16 either untreated (Control), treated with AA (AA), or a combination of AA and MG132 (AAMG), as described in Fig. 3A. We used FLAG-tagged beads for co-IP, followed by on-bead trypsin digestion and LC-MS/MS.

To provide an in-depth analysis into the effects of AA on the E6 interactome and perform quality control on the experiment, we performed database searches using both MaxQuant and FragPipe and filtered the datasets as follows: we removed reverse sequences, potential contaminants and proteins only identified by site; we filtered the data to retain proteins with at least three valid values in one experimental group \, followed by $\log_2$ transformation. Overall, we identified over 1100 proteins per sample group in the MaxQuant dataset (Fig. S2A), and more than 1290 proteins using FragPipe (Fig. S2B). While the total number of proteins identified varied, most likely due to differences in the search algorithms, both databases exhibited similar profiles. Notably, AA-treated samples showed the highest number of identified proteins. However, AA+MG132 samples displayed a similar number of identified proteins as untreated samples, and lower than AA-treated samples. This could suggest a potential issue with our MG132 treatment, since the inhibition of proteasomal degradation should have led to an accumulation of proteins. Nonetheless, the MG132 dataset was kept, as MG132 can still provide important information by stabilizing short-lived or degradation-prone proteins. To further validate the efficiency of our co-IP approach, we examined the presence of E6AP, a well-established interactor of E6, in our dataset. We could confirm that E6AP was significantly enriched in E6-expressing samples, which confirms the effectiveness of our co-IP in enriching E6 interactors and indicates that AA treatment does not disrupt all E6 interactions (Fig. S2C-D). A closer inspection of the overlap between sample groups revealed that the majority of proteins were shared across treatments. Nevertheless, in the MaxQuant dataset, we identified 68 proteins that are unique to AA treatment, 3 to AA+MG132 and 18 shared between these treatments (Fig. S2E). With FragPipe dataset, we showed 43 proteins specific to AA-only samples, 5 in AA+MG132 and 55 proteins shared between AA and AA+MG132 (Fig. S2F). These findings point to AA-dependent changes to the E6 interactome.

After the first filtering, we imputed the missing values from a normal distribution based on total matrix (0.3 width, 1.8 down shift), to ensure a balanced dataset for downstream analysis. Manual inspection of a random selection of rows was performed to ensure the imputation was not altering the data. Principal component analysis (PCA) showed distinct clustering of samples based on the treatment conditions (Fig. 3B). The proximity of replicates within each treatment highlights the consistency and reproducibility of our experimental approach. The separation between treatments indicates distinct variations in the E6 interactome in response to AA and AA+MG132 treatments when compared to the controls. To further characterize treatment-dependent protein enrichments, we performed hierarchical clustering of z-scored ANOVA-significant imputed data (Fig. 3C). Notably, three distinct proteins clusters were identified: a cluster with proteins enriched in AA-treated samples, which includes proteins involved in mRNA splicing, translation, ubiquitin-dependent protein catabolic processes, and proteasomal protein catabolic processes; a second cluster of proteins enriched in the negative control, pWPI, serving as a baseline to filter out background proteins from downstream analysis; and a final cluster of proteins enriched in AA+MG132-treated samples, associated with biological processes including positive regulation of ubiquitin protein ligase activity, RNA splicing and processing, ribonucleoprotein complex biogenesis and chromosome organization. These findings are noteworthy, as they provide valuable insights into the biological processes modulated by AA treatment. The enrichment of proteins involved in ubiquitin-dependent and proteasomal catabolic processes and proteasomal protein catabolic processes in AA-treated samples aligns with our previous observations that AA induces E6 ubiquitination and subsequent degradation. Furthermore, the enrichment of processes such as mRNA splicing and translation may imply that AA treatment leads to new interactions that help mitigate oncogenic stress induced by E6. Additionally, the presence of proteins associated with the positive regulation of ubiquitin protein ligase activity in AA+MG132 conditions align with the proteasomal inhibition caused by the presence of MG132, thereby validating its use in our experimental framework. The presence of processes like ribonucleoprotein complex biogenesis and chromosome organization may also provide mechanistic insights into the increased cell death observed in the cells following AA treatment.

Next, to further interrogate the dataset, we used a series of volcano plots to provide a comprehensive overview of potential E6 interactors across treatment conditions. Each volcano plot displays potential interactors of E6 across the various treatment conditions. The significance of each possible interactor is determined through a permutation-based false discovery rate (FDR), which results in high-confidence Class A (solid line) and low-confidence Class B (dashed lines) thresholds (Fig. S3). These findings show that under Control conditions, no Class A or B interactors were detected, with the sole exception being our bait (E6 protein). Although both AA and AA+MG132 conditions identified Class A and Class B interactions, AA+MG132 identified a single protein, NUMA1, as a Class A interactor, a microtubule-associated protein. In contrast, the AA condition identified more than 400 Class A interactors, including multiple proteasomal subunits, such as PSMA1–7, PSMB1–7, PSMC1–6 and PSMD1–14, along with additional proteins associated with the proteasome complex. This observation is particularly compelling, as these proteasomal subunits were not significantly enriched under control or AA+MG132 conditions, where MG132 was used to block proteasomal degradation. Since proteasomal degradation is blocked by MG132, it is expected that E6 will not be processed by proteasomal proteins, which explains the absence of proteasomal subunit enrichment. Thus, this finding supports our hypothesis regarding AA's role in mediating E6 proteasomal degradation. Additionally, a few E3 ligases were also classified as Class A and Class B under AA and AA+MG132 treatment conditions. For instance, TRIP12 is highlighted in AA samples, whereas SKP1 and CDC20 emerge as significant candidates in AA+MG132 condition. This underscores the utility of proteasomal inhibition in uncovering E6 interactions that may otherwise remain undetected, highlighting the importance of this methodological approach in elucidating E6's functional interactome. Importantly, a study investigating the sensitivity of HPV-positive head and neck squamous cell carcinoma (HNSCC) to radiotherapy reported that TRIP12 is downregulated and is controlled by p16, leading to G1 cell cycle arrest and impaired DNA repair [41,42]. This could explain how TRIP12 was only identified in AA samples and raises the question of whether the presence of AA could affect the p16-TRIP12 relationship, so that TRIP12 is used to target E6 for degradation instead. Additionally, the SCF^{Skp2} ubiquitin ligase complex, of which SKP1 is a core component, was reported to target the HPV18 E2 protein, allowing for a higher E6 and E7 expression [43]. HPV E2 expression is important for viral replication and transcription at the early stages by controlling E6 and E7

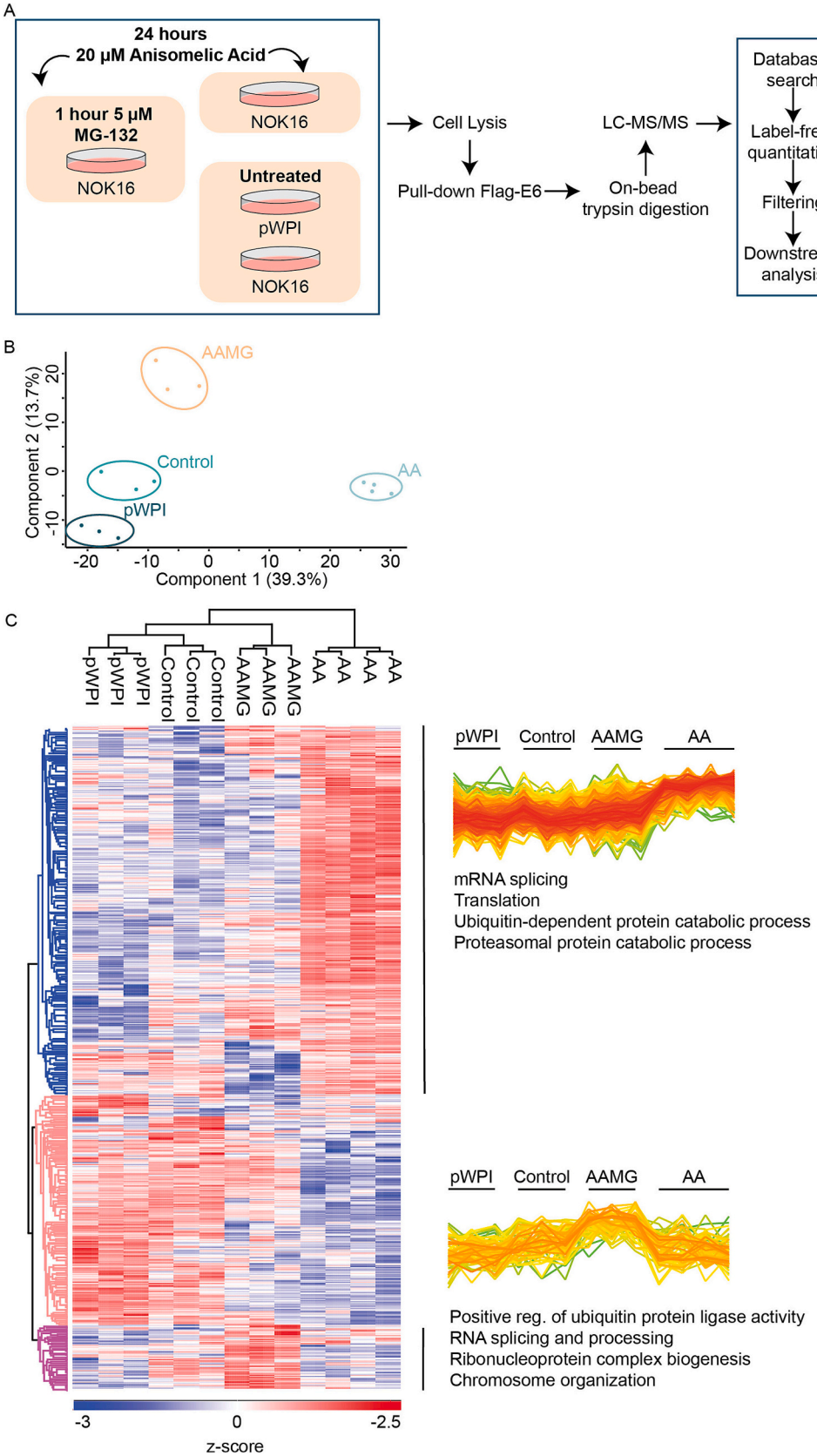

Fig. 3. Imputed data analysis reveals enrichment of ubiquitin dependent and proteasomal processes in AA-treated samples. a) Model of the experimental methodology employed for our interactome study. b) Principal component analysis of all samples in this dataset. c) Hierarchical clustering was performed on imputed ANOVA significant z-scored data. Each row represents individual proteins, while each column corresponds to different samples. An enrichment analysis of the highlighted row clusters was executed based on biological processes using ShinyGo 0.80.

transcription, but is repressed in HPV-positive cancers [44,45]. Although E2 and E6 proteins do not share similarities sequence-wise, the fact that the SCF^{Skp2} ubiquitin ligase has been shown to interact with other HPV proteins makes it an attractive candidate for E6 targeting. Notably, CDC20, an activator of the APC/C E3 ligase, also binds to HPV E2 proteins. In this case, it leads to genomic instability in high-risk HPVs [46,47]. Given its established interaction with another HPV protein, CDC20 represents another plausible candidate for supporting E6 degradation.

In summary, AA treatment reshapes the E6 interactome by enriching proteasomal and ubiquitin-related proteins, while MG132 inhibition refines E6-associated interactions. These findings support our hypothesis that AA promotes E6 degradation, consistent with our earlier experimental results. Additionally, several E3 ligase candidates were identified, warranting future biochemical validation. While analysis of the E6 interactome provided useful information on the enriched proteins, this presents challenges for downstream interpretation. To address this, we implemented a filtering strategy to narrow down the list and focus on the most biologically relevant proteins.

3.3. Filtering of the E6 interactome identifies specific E3 ligases and RAD23B

Despite the important insights provided by analyzing the E6 interactome dataset as a whole, the number of possible interactors of E6 was too high to dissect. Therefore, to gain further insights from our datasets, we decided to exclude proteins that exhibited higher levels in pWPI than in NOK16 samples (Fig. 3C, cluster 2), by using a ratio of NOK16/pWPI greater than 1.05 as a cut-off, resulting in a more concise list that facilitated downstream analysis. As quality control, we cross-referenced our data against CRAPome, a database which collects proteins that are frequently identified as contaminants in affinity purification-mass spectrometry experiments. Notably, our findings indicate that most of our identified proteins are not common contaminants in affinity purification MS studies (Fig. 4A and S4A). This observation reinforces the specificity of the identified candidates, thereby enhancing the significance of our results. Then, we did a gene ontology analysis that revealed a markedly distinct profile of the top 10 enriched biological processes when comparing treatment conditions (Fig. 4B and S4B). Although proteasomal and ubiquitin-related processes were enriched in all conditions, we noticed that one of the enriched biological processes observed following AA treatment in the MaxQuant dataset is “response to heat”, while chaperone-mediated protein folding was noted in Fragpipe’s AA+MG132 dataset, suggesting the involvement of potential stress-related cellular mechanisms.

Our ratio cut-off resulted in a list comprising 160 proteins with MaxQuant (Fig. 4C). In particular, 19 across all samples, 41 unique to AA, 3 unique to AA+MG132 and 18 proteins that are enriched in both AA and AA+MG132 conditions (Fig. 4C). On the other hand, with Fragpipe we observed 190 proteins (Fig. S4C), specifically 20 proteins in all samples, 43 unique to AA, 5 unique to AA+MG132 and 45 proteins that are enriched in both conditions (Fig. S4C). Importantly, both methodologies revealed distinct proteins of interest associated with protein degradation pathways. For instance, E6AP and UBR4 were found across all samples, which is expected, as reports exist on their involvement in HPV-positive cancers. E6AP is mostly known for forming a complex with HPV E6 and p53, which results in the ubiquitination and degradation of p53 [48]. Its spatial proximity to E6 makes it a good candidate for E6 ubiquitination. Thus, it is possible that AA binding to E6 could lead to a conformational change that would make E6 more susceptible to ubiquitination by E6AP, rather than p53. Although no previous evidence suggests an interaction between UBR4 and E6, this is a noteworthy candidate as it binds HPV E7 and directs PTPN14, a protein that may function as a tumor suppressor, for degradation [40,49]. This could suggest that UBR4 could extend its substrate range to E6, as it has been reported that E6 and E7 can directly bind to each other [50]. Two other proteins related to protein degradation are PJA2 in AA-only samples and RAD23B in NOK16 samples. PJA2 is usually involved in PKA-mediated processes but has recently been reported to mediate the degradation of HDAC2, which helps with inhibiting tumor progression in colorectal cancer [51,52]. No evidence of its involvement with HPV-positive cancers has been reported yet.

While not an E3 ligase like the previously mentioned proteins, RAD23B can bind ubiquitinated substrates and deliver them to the proteasome for degradation [53]. This protein was found in all NOK16 samples and could provide further information on E6 degradation and how it is transported to the proteasome. Moreover, with MaxQuant we found CBLL1, CDC20 and SKP1 in NOK16 samples. CBLL1 is associated with tumor progression and epithelial-to-mesenchymal transition [54,55]. While its role in cancer is evident, no direct evidence has been found of a possible role in HPV-positive cancers. Furthermore, its main activity is associated with pro-tumor roles. While using FragPipe, we identified TRIM26 in AA-only samples. TRIM26 possesses both oncogenic (in bladder and non-small cell lung cancer) and tumor-suppressive (gastric and clear cell renal cell carcinoma) roles, depending on the cancer type [56–59]. A connection to HPV-positive cancer has not been reported yet. However, due to its multifaceted roles in different organs, its involvement with E6 ubiquitination cannot be overlooked.

Our non-imputed, filtered data analysis shows enrichment of proteins related to degradation and ubiquitin pathway. Furthermore, our results underscore the complementary nature of the pipelines, demonstrating their capacity to yield overlapping results alongside unique potential interactors of E6. They provided us with multiple possible candidates that would benefit from investigating their interaction with E6. This could be approached by inhibition of the E3 ligases to access direct binding to E6 and E6 ubiquitin levels. To refine our candidate selection, we decided to integrate multiple complementary approaches to better prioritize which interactions to investigate further.

3.4. Comparative analysis of data processing pipelines and sequence analysis pinpoint UBR4, E6AP, CDC20 and TRIP12 as strong candidates

Due to multiple available approaches for analyzing MS data, we sought to compare different stages of our analytical pipeline, with the objective of identifying key interactors of E6. Network 1 represented initial preprocessing for our data, which included contaminant removal and initial filtering for valid values. From there, we built network 2 from imputed ANOVA-significant z-scored data; and for the final matrix, we filtered out proteins with a NOK16/pWPI ratio smaller than 1.05. Analysis of these three networks revealed that, using either MaxQuant or FragPipe, the three have less than 20 proteins in common (Fig. 5A). Most proteins were consistently identified in at least two networks. From this analysis we were able to highlight several proteins implicated in proteasomal degradation, including multiple E3 ligases, such as TRIM28, TRIP12, CBLL1, PJA2, SKP1, E6AP and UBR4, along with RAD23B, a shuttle protein that transports ubiquitinated proteins to the proteasome for degradation. The strong overlap between MaxQuant and FragPipe approaches underscores their reliability in identifying high-confidence interactors.

Finally, to further enhance the robustness and depth of our data analysis, we utilized the Significance Analysis of Interactome (SAINT), which focuses on interactome analysis to distinguish true interactors from nonspecific binders [24]. We filtered the data by SAINT score (SP) > 2, FCA > 2 and minimum abundance of 1.5. Then, we cross-reference the results against our previous analysis (Fig. 5B). This approach highlighted key E3 ligases including CDC20, E6AP and UBR4 in all samples, and PJA2, which was identified exclusively in AA-treated samples. We also saw RAD23B in all groups, in addition to members of the proteasome PSMD13, PSMB5 and PSMD7, which is in line with E6 degradation via the proteasomal pathway. The consistent detection of E3 ligases across multiple conditions and analytical pipelines points to several possible regulators of E6 AA-mediated degradation. While PJA2 was the

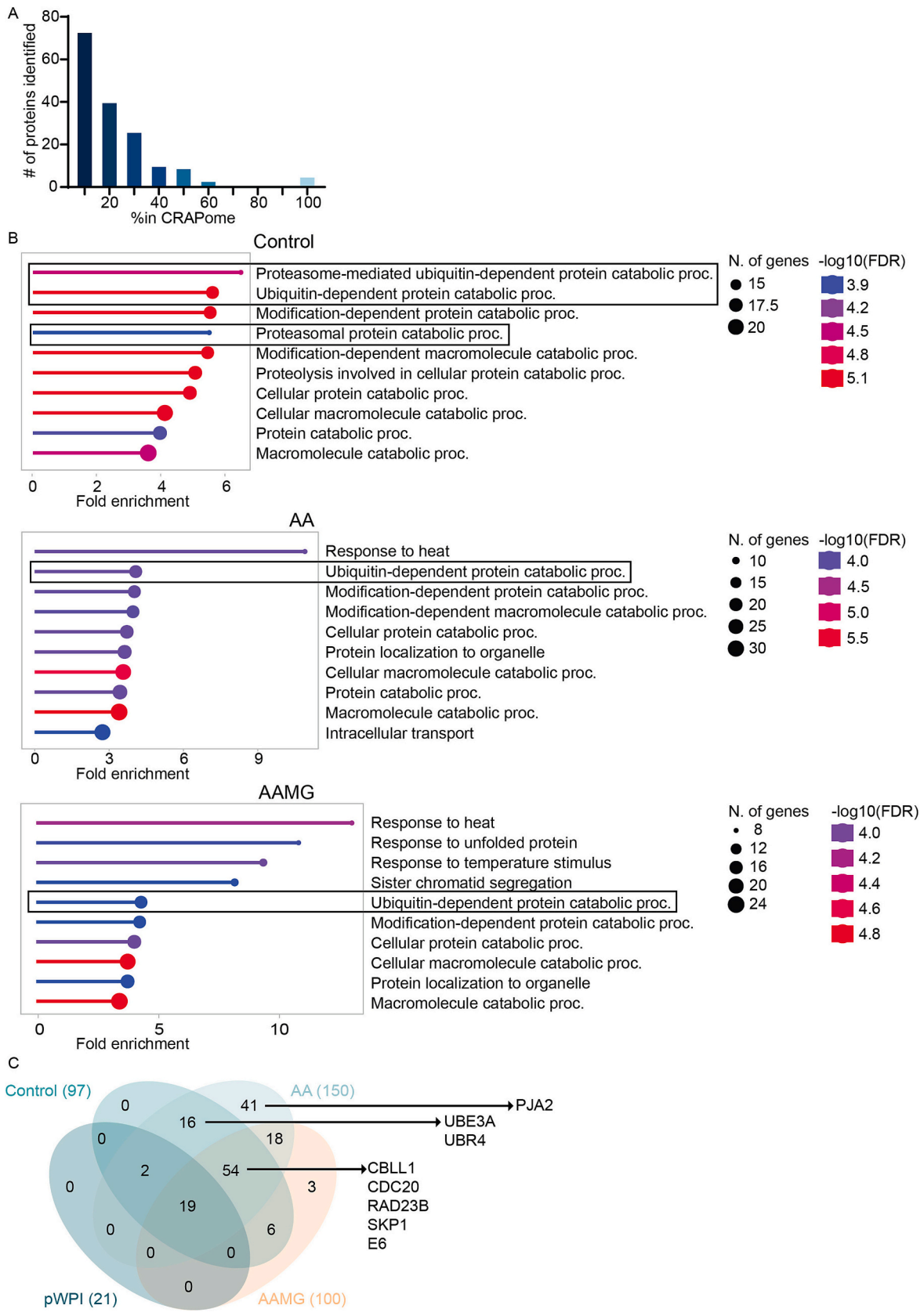

Fig. 4. MaxQuant and Perseus data analysis identify enriched proteins related to degradation and ubiquitin pathways in NOKs 16. a) Bar graph illustrating how frequently the proteins in this dataset appear in a contaminant database (CRAPome). b) Chart representing the GO biological processes that are enriched in each treatment type. The size of the circles represents the number of genes identified in each biological process, in a treatment group, whereas the color of the bars represents the -log10(FDR) values. c) Venn diagram comparing the identified proteins between samples, after filtering out NOK16/pWPI ratio smaller than 1.05.

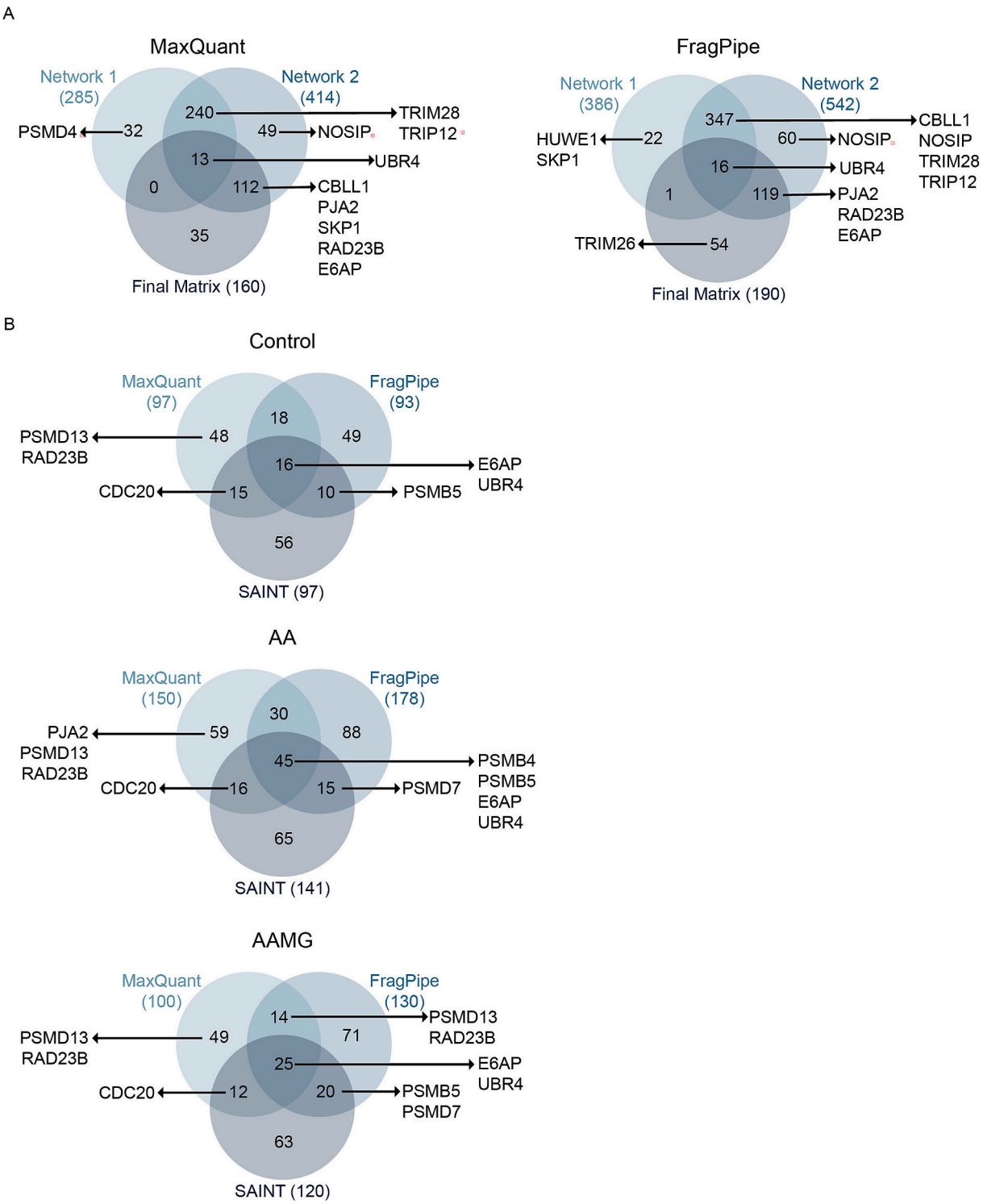

Fig. 5. Comparative study of different analytical pipelines consistently detects different E3 ligases and proteasomal subunits. a) Venn diagram compares the different networks and matrices obtained at different stages of the MaxQuant (top) and FragPipe (bottom) analysis. Network 1 was obtained from the initial preprocessing of the data. Network 2 was generated from imputed ANOVA-significant z-scored data. Final matrix was obtained by filtering out proteins with a NOK16/pWPI ratio smaller than 1.05. b) Venn diagram comparing MaxQuant, FragPipe and SAINT across different sample conditions: Control (top), AA (middle) and AA+MG132 (bottom). Final matrices were used for the MaxQuant and FragPipe datasets.

sole E3 ligase exclusively identified in AA-treated samples, rendering it a compelling candidate for further validation, other E3 ligases equally merit consideration as viable candidates to target E6 for degradation. As our findings indicate, there is direct interaction between AA and E6, which may induce a conformational alteration of the E6 structure. This conformational change could enhance its susceptibility to ubiquitination, thereby facilitating E3 ligases, which normally bind to E6, to conjugate ubiquitin to E6, thus marking it for proteasomal degradation. Furthermore, the repeated identification of RAD23B and proteasomal subunits as E6 interactors could provide additional insight into the degradation of E6, as RAD23B may play a pivotal role in the transportation of E6 to the proteasome.

The HPV E6 protein is known to interact with host proteins using two distinct interfaces. First, at its C-terminus, E6 contains a PDZ-binding domain motif (PBM) with a sequence of SSRTRRETQL. This PBM mediates interactions with PDZ domain–containing proteins such as hDlg and Scribble, contributing to disruption of cell polarity and oncogenic transformation [60,61]. Second, E6 possesses a hydrophobic pocket that can recognize host proteins containg LxxLL motifs [62]. As previously reported, E6AP binds to E6 via the LxxLL-motif [63]. To explore whether similar mechanisms could be the basis of interactions with the E3 ligases identified in our study, we performed sequence analysis to examine the presence of PDZ domains and LxxLL motifs. None of the E3 ligases analyzed contained PDZ domains, making interactions through E6's PDZ-binding motif unlikely. In contrast, several ligases possessed LxxLL motifs: UBR4 (24 instances in isoform 1), TRIP12 (four instances) and CDC20 (one instance). The presence of these motifs supports the possibility of direct interaction with E6 via its LxxLL-binding pocket, thus making them compelling targets for further investigation as E6-interacting partners. Future studies could prioritize in silico structural modelling of E6-E3 ligase interactions to predict binding interfaces and affinities, followed by biochemical validation using co-immunoprecipitation or site-directed mutagenesis of predicted binding regions.

To further evaluate the plausibility of E6 interactions with the candidate E3 ligases, we considered the biological pathways in which these ligases function. It is well documented that E6 binds E6AP to target p53 for degradation. The presence of AA could interfere with this interaction, potentially redirecting E6AP activity toward E6 itself. Our previous findings show that AA treatment stabilizes p53 while downregulating E6, which would support the hypothesis that E6AP may facilitate the degradation of E6 in the presence of AA. UBR4 also presents itself as a compelling candidate, due to its association with E7 for PTPN14 degradation [64]. In our proteomics analysis, UBR4 is identified as a potential interactor of E6. Furthermore, we have observed that both E6 and E7 are downregulated after AA treatment in HPV-positive cancer cells [13]. Recent reports of direct E6-E7 interaction [50] raise the possibility that UBR4 may mediate the degradation of both oncoproteins. Such dual targeting could contribute to the rapid stabilization of key targets like p53 and p21, and to the activation of the apoptotic signaling observed after AA treatment. TRIP12 also warrants consideration, as it contains LxxLL motifs that could facilitate its binding to E6. It has been shown to interact with USP7, a deubiquitinase involved in DNA damage response through p53 stabilization. This TRIP12-USP7 interaction enables reciprocal regulation of expression [65]. In HPV-associated cancers, USP7 is reported to stabilize E7, thereby contributing to HPV carcinogenesis [66]. These observations suggest a possible mechanism by which E6 could modulate E7 expression indirectly through the TRIP12-USP7 axis, a regulatory relationship that may also be perturbed by AA. CDC20, a key co-activator of the anaphase promoting complex/cyclosome (APC/C), was also among the E3 ligases identified in our dataset containing an LxxLL motif. Previous studies have shown that, in high-risk HPV infections, HPV E2 protein interacts with CDC20 to promote genomic instability [46]. In addition, CDC20 is upregulated in HPV-positive cancer cells due to E6 and E7 disruption of p53 and pRB functions [47]. Although E2 and E6 do not share significant sequence homology, E6 could use the LxxLL-motif to bind to CDC20, potentially enabling further control over cell cycle progression by modulating APC/C activity and cyclin B degradation. Given our hypothesis that AA binding induces a conformational change in E6, it is conceivable that this altered structure could redirect CDC20's activity toward E6 itself, leading to its degradation in place of its typical cell cycle targets.

By integrating multiple analysis pipelines with sequence motif analysis, we have pinpointed UBR4, E6AP, CDC20 and TRIP12 as strong candidates involved in AA-mediated degradation of E6. These E3 ligases not only contain LxxLL motifs, supporting the possibility of direct interaction with E6, but also function in pathways that would be advantageous for HPV-positive cancer cells to manipulate. Further studies, including in silico structural modelling and biochemical validation, are necessary to elucidate their precise roles in mediating E6 degradation.

4. Conclusions

In this study, we employed MS-based proteomics approach to investigate how anisomelic acid induces the ubiquitination and proteasomal degradation of the HPV16 E6 oncoprotein. Through cellular assays, we demonstrated that AA increases E6 ubiquitination, which explains the decrease of E6 levels observed in our previous study. Additionally, CETSA data provides compelling evidence for a potential direct interaction of AA and E6, suggesting that AA binding may induce a conformational change, which increases E6's susceptibility to ubiquitination. Future studies investigating the binding affinity and kinetics of the AA–E6 interaction will be essential for optimizing its therapeutic potential and guiding the design of AA-derived small molecules.

Our MS approach identified several E3 ligases, such as TRIM28, TRIP12, CDC20, CBLL1, PJA2, SKP1, E6AP and UBR4, highlighting their potential roles in AA-mediated E6 degradation. Although each of the identified E3 ligases mentioned here appears to be a good candidate, TRIP12, CDC20, E6AP and UBR4 could be considered the most probable interaction partner of E6, due to their proximity with HPV E6 and/or other HPV proteins and possessing a LxxLL-motif, which could be used for direct binding with E6. Furthermore, the repeated identification of the shuttle protein RAD23B underscores its potential involvement in delivering ubiquitinated E6 to the proteasome to be degraded. By comparing the results obtained with MaxQuant, FragPipe and SAINT, we demonstrated the complementary nature that provide a more robust identification of high-confidence E6 interactors. By focusing on proteins consistently detected across different pipelines, we have identified different components of the ubiquitin-proteasome system, including proteasomal subunits PSMD13, PSMB5, and PSMD7, which may further explain the precise degradation pathway of E6. Together, these findings support a working model in which AA binding induces conformational change of E6, facilitating its recognition by specific E3 ligases, ubiquitination, and subsequent delivery by the shuttle protein RAD23B to the proteasome for degradation. While this model integrates our key observations, further validation through biochemical assays is essential to confirm the roles of the candidate E3 ligases and proteasomal components in this pathway. Importantly, our findings reveal that AA not only disrupts E6 function but also modulates the E6 interactome, enriching biological processes associated with protein degradation, mRNA splicing, and stress response pathways. These observations suggest that AA exerts multifaceted effects on cellular processes, potentially mitigating the oncogenic stress induced by E6, which leads to cells death of HPV-positive cancer cells.

In conclusion, this study provides the first comprehensive proteomics framework of the HPV16 E6 interactome under pharmacological perturbation. Beyond offering mechanistic insight into AA-mediated degradation of E6, the dataset itself constitutes a significant resource for the HPV field. These findings pave the way for the development of AA-like small molecules as targeted therapeutic strategies for HPV-positive cancers, potentially offering a safer and more specific alternative to conventional treatments. While functional validation of individual ligases and proteasomal components is ongoing, timely dissemination of this work provides immediate value for the field and work related to developing targeted therapies to address HPV-mediated diseases.

Supplementary data to this article can be found online at https://doi.org/10.1016/j.jprot.2025.105536.

Significance

This study explores AA as a potential therapeutic strategy against

HPV-positive cells. We reveal that AA directly interacts with HPV16 E6, increases its ubiquitination, which facilitates its degradation. Through affinity purification-mass spectroscopy and by integrating proteomics analysis pipelines with sequence motif analysis, we identified strong potential candidates mediating AA-induced E6 degradation. This work not only advances our understanding of AA's mechanism of action but also provides a basis for further exploration of these candidate proteins as E6-degradation mediators.

CRediT authorship contribution statement

Michael Santos Silva: Writing – review & editing, Writing – original draft, Visualization, Methodology, Investigation, Formal analysis, Data curation, Conceptualization. **Leila S. Coelho-Rato:** Writing – review & editing, Writing – original draft, Visualization, Methodology, Investigation, Formal analysis, Data curation. **Navid Delshad:** Writing – review & editing, Investigation. **Tatiana Tarkhova:** Investigation. **Joakim Edman:** Investigation. **Preethy Paul:** Writing – review & editing, Supervision, Funding acquisition. **Annika Meinander:** Writing – review & editing, Supervision. **John E. Eriksson:** Writing – review & editing, Supervision, Funding acquisition, Conceptualization.

Declaration of competing interest

MSS, LSCR, ND, TT, JE and AM declare no conflict of interest. PP and JEE are co-founders of Anison Therapeutics Oy, a start-up company which holds patents for the pharmaceutical compositions of AA and the use thereof. This affiliation could be perceived as a potential conflict of interest due to the commercial implications of the findings of this manuscript. All authors followed rigorous scientific and ethical standards to ensure accurate and unbiased results.

Acknowledgments

We would like to thank the Jane Ja Aatos Erko Foundation, the Cancer Foundation Finland, Ida Montinin Säätiö and The Maud Kuistila Memorial Foundation for the funding. Åbo Akademi University, and the Turku Bioscience Centre and Biocenter Finland for the research facilities. This research was also supported by InFLAMES Flagship Programme of the Academy of Finland (decision numbers: 337531, 357911).

Data availability

The mass spectrometry proteomics data have been deposited to the ProteomeXchange Consortium via the PRIDE [67] partner repository with the dataset identifier PXD065382.

References

[1] N. Muñoz, F.X. Bosch, S. De Sanjosé, R. Herrero, X. Castellsagué, K.V. Shah, P.J. F. Snijders, C.J.L.M. Meijer, Epidemiologic classification of human papillomavirus types associated with cervical cancer, N. Engl. J. Med. 348 (2003) 518–527, https://doi.org/10.1056/NEJMoa021641.

[2] L.L.D. Silva, A.M. Teles, J.M.O. Santos, M. Souza De Andrade, R. Medeiros, A. I. Faustino-Rocha, P.A. Oliveira, A.P.A. Dos Santos, F. Ferreira Lopes, G. Braz, H. O. Brito, R.M.G.D. Costa, Malignancy associated with Low-risk HPV6 and HPV11: a systematic review and implications for cancer prevention, Cancers 15 (2023) 4068, https://doi.org/10.3390/cancers15164068.

[3] A.M. Filho, M. Laversanne, J. Ferlay, M. Colombet, M. Piñeros, A. Znaor, D. M. Parkin, I. Soerjomataram, F. Bray, G.L.O.B.O.C.A.N. The, cancer estimates: data sources, methods, and a snapshot of the cancer burden worldwide, Int. J. Cancer 156 (2025) (2022) 1336–1346, https://doi.org/10.1002/ijc.35278.

[4] J. Ferley, M. Ervik, F. Lam, M. Laversanne, M. Colombet, L. Mery, M. Piñeros, A. Znaor, I. Soerjomataram, F. Bray, Global Cancer Observatory: Cancer Today. https://gco.iarc.who.int/today, 2024 (accessed January 2, 2024).

[5] J.E. Jensen, G.L. Becker, J.B. Jackson, M.B. Rysavy, Human papillomavirus and associated cancers: a review, Viruses 16 (2024) 680, https://doi.org/10.3390/v16050680.

[6] L. Bruni, G. Albero, B. Serrano, M. Mena, J. Collado, D. Gómez, J. Muñoz, F. Bosch, S. De Sanjosé, ICO/IARC information Centre on HPV and Cancer (HPV Information Centre), Human Papillomavirus and Related Diseases in the World., Summary Report 10 March 2023. https://hpvcentre.net/statistics/reports/XWX.pdf?t=1739279264773, 2023.

[7] J. Doorbar, W. Quint, L. Banks, I.G. Bravo, M. Stoler, T.R. Broker, M.A. Stanley, The biology and life-cycle of human papillomaviruses, Vaccine 30 (2012) F55–F70, https://doi.org/10.1016/j.vaccine.2012.06.083.

[8] X. Bernard, P. Robinson, Y. Nominé, M. Masson, S. Charbonnier, J.R. Ramirez-Ramos, F. Deryckere, G. Travé, G. Orfanoudakis, Proteasomal degradation of p53 by human papillomavirus E6 Oncoprotein relies on the structural integrity of p53 Core domain, PLoS One 6 (2011) e25981, https://doi.org/10.1371/journal.pone.0025981.

[9] B.A. Werness, A.J. Levine, P.M. Howley, Association of human papillomavirus types 16 and 18 E6 proteins with p53, Science (1990), https://doi.org/10.1126/science.2157286.

[10] C.A. Moody, L.A. Laimins, Human papillomavirus oncoproteins: pathways to transformation, Nat. Rev. Cancer 10 (2010) 550–560, https://doi.org/10.1038/nrc2886.

[11] K. Münger, B.A. Werness, N. Dyson, W.C. Phelps, E. Harlow, P.M. Howley, Complex formation of human papillomavirus E7 proteins with the retinoblastoma tumor suppressor gene product, EMBO J. 8 (1989) 4099–4105, https://doi.org/10.1002/j.1460-2075.1989.tb08594.x.

[12] J.C. Romero-Masters, P.F. Lambert, K. Munger, Molecular mechanisms of MmuPV1 E6 and E7 and implications for human disease, Viruses 14 (2022) 2138, https://doi.org/10.3390/v14102138.

[13] P. Paul, S.K. Rajendran, E. Peuhu, A.A. Alshatwi, M.A. Akbarsha, S. Hietanen, J. E. Eriksson, Novel action modality of the diterpenoid anisomelic acid causes depletion of E6 and E7 viral oncoproteins in HPV-transformed cervical carcinoma cells, Biochem. Pharmacol. 89 (2014) 171–184, https://doi.org/10.1016/j.bcp.2014.02.011.

[14] R. Yang, J. Klimentová, E. Göckel-Krzikalla, R. Ly, N. Gmelin, A. Hotz-Wagenblatt, H. Řehulková, J. Stulík, F. Rösl, M. Niebler, Combined transcriptome and proteome analysis of immortalized human keratinocytes expressing human papillomavirus 16 (HPV16) oncogenes reveals novel key factors and networks in HPV-induced carcinogenesis, mSphere 4 (2019) e00129–19, https://doi.org/10.1128/mSphere.00129-19.

[15] J. Cox, M. Mann, MaxQuant enables high peptide identification rates, individualized p.p.b.-range mass accuracies and proteome-wide protein quantification, Nat. Biotechnol. 26 (2008) 1367–1372, https://doi.org/10.1038/nbt.1511.

[16] J. Cox, M.Y. Hein, C.A. Luber, I. Paron, N. Nagaraj, M. Mann, Accurate proteome-wide label-free quantification by delayed normalization and maximal peptide ratio extraction, termed MaxLFQ*, Mol. Cell. Proteomics 13 (2014) 2513–2526, https://doi.org/10.1074/mcp.M113.031591.

[17] F. da Veiga Leprevost, S.E. Haynes, D.M. Avtonomov, H.-Y. Chang, A. K. Shanmugam, D. Mellacheruvu, A.T. Kong, A.I. Nesvizhskii, Philosopher: a versatile toolkit for shotgun proteomics data analysis, Nat. Methods 17 (2020) 869–870, https://doi.org/10.1038/s41592-020-0912-y.

[18] A.T. Kong, F.V. Leprevost, D.M. Avtonomov, D. Mellacheruvu, A.I. Nesvizhskii, MSFragger: ultrafast and comprehensive peptide identification in mass spectrometry–based proteomics, Nat. Methods 14 (2017) 513–520, https://doi.org/10.1038/nmeth.4256.

[19] F. Yu, S.E. Haynes, A.I. Nesvizhskii, IonQuant enables accurate and sensitive label-free quantification with FDR-controlled match-between-runs, Mol. Cell. Proteomics 20 (2021) 100077, https://doi.org/10.1016/j.mcpro.2021.100077.

[20] S. Tyanova, T. Temu, P. Sinitcyn, A. Carlson, M.Y. Hein, T. Geiger, M. Mann, J. Cox, The Perseus computational platform for comprehensive analysis of (prote) omics data, Nat. Methods 13 (2016) 731–740, https://doi.org/10.1038/nmeth.3901.

[21] H. Heberle, G.V. Meirelles, F.R. da Silva, G.P. Telles, R. Minghim, InteractiVenn: a web-based tool for the analysis of sets through Venn diagrams, BMC Bioinform. 16 (2015) 169, https://doi.org/10.1186/s12859-015-0611-3.

[22] S.X. Ge, D. Jung, R. Yao, ShinyGO: a graphical gene-set enrichment tool for animals and plants, Bioinformatics 36 (2020) 2628–2629, https://doi.org/10.1093/bioinformatics/btz931.

[23] D. Mellacheruvu, Z. Wright, A.L. Couzens, J.-P. Lambert, N. St-Denis, T. Li, Y. V. Miteva, S. Hauri, M.E. Sardiu, T.Y. Low, V.A. Halim, R.D. Bagshaw, N.C. Hubner, A. Al-Hakim, A. Bouchard, D. Faubert, D. Fermin, W.H. Dunham, M. Goudreault, Z.-Y. Lin, B.G. Badillo, T. Pawson, D. Durocher, B. Coulombe, R. Aebersold, G. Superti-Furga, J. Colinge, A.J.R. Heck, H. Choi, M. Gstaiger, S. Mohammed, I. M. Cristea, K.L. Bennett, M.P. Washburn, B. Raught, R.M. Ewing, A.-C. Gingras, A. I. Nesvizhskii, The CRAPome: a contaminant repository for affinity purification mass spectrometry data, Nat. Methods 10 (2013) 730–736, https://doi.org/10.1038/nmeth.2557.

[24] H. Choi, B. Larsen, Z.-Y. Lin, A. Breitkreutz, D. Mellacheruvu, D. Fermin, Z.S. Qin, M. Tyers, A.-C. Gingras, A.I. Nesvizhskii, SAINT: probabilistic scoring of affinity purification-mass spectrometry data, Nat. Methods 8 (2011) 70–73, https://doi.org/10.1038/nmeth.1541.

[25] S. Berg, D. Kutra, T. Kroeger, C.N. Straehle, B.X. Kausler, C. Haubold, M. Schiegg, J. Ales, T. Beier, M. Rudy, K. Eren, J.I. Cervantes, B. Xu, F. Beuttenmueller, A. Wolny, C. Zhang, U. Koethe, F.A. Hamprecht, A. Kreshuk, Ilastik: interactive machine learning for (bio)image analysis, Nat. Methods 16 (2019) 1226–1232, https://doi.org/10.1038/s41592-019-0582-9.

[26] J. Schindelin, I. Arganda-Carreras, E. Frise, V. Kaynig, M. Longair, T. Pietzsch, S. Preibisch, C. Rueden, S. Saalfeld, B. Schmid, J.-Y. Tinevez, D.J. White, V. Hartenstein, K. Eliceiri, P. Tomancak, A. Cardona, Fiji: an open-source platform

for biological-image analysis, Nat. Methods 9 (2012) 676–682, https://doi.org/10.1038/nmeth.2019.
[27] D.R. Stirling, M.J. Swain-Bowden, A.M. Lucas, A.E. Carpenter, B.A. Cimini, A. Goodman, CellProfiler 4: improvements in speed, utility and usability, BMC Bioinform. 22 (2021) 433, https://doi.org/10.1186/s12859-021-04344-9.
[28] S. Li, X. Hong, Z. Wei, M. Xie, W. Li, G. Liu, H. Guo, J. Yang, W. Wei, S. Zhang, Ubiquitination of the HPV Oncoprotein E6 is critical for E6/E6AP-mediated p53 degradation, Front. Microbiol. 10 (2019), https://doi.org/10.3389/fmicb.2019.02483.
[29] K. Jing, S. Shin, S. Jeong, S. Kim, K.-S. Song, J.-H. Park, J.-Y. Heo, K.-S. Seo, S.-K. Park, G.-R. Kweon, T. Wu, J.-I. Park, K. Lim, Docosahexaenoic acid induces the degradation of HPV E6/E7 oncoproteins by activating the ubiquitin–proteasome system, Cell Death Dis. 5 (2014) e1524, https://doi.org/10.1038/cddis.2014.477.
[30] R. Jafari, H. Almqvist, H. Axelsson, M. Ignatushchenko, T. Lundbäck, P. Nordlund, D.M. Molina, The cellular thermal shift assay for evaluating drug target interactions in cells, Nat. Protoc. 9 (2014) 2100–2122, https://doi.org/10.1038/nprot.2014.138.
[31] R. Senthilkumar, Y. Brusentsev, P. Paul, P. Marimuthu, F. Cheng, P.C. Eklund, J. E. Eriksson, Synthesis and evaluation of Anisomelic acid-like compounds for the treatment of HPV-mediated carcinomas, Sci. Rep. 9 (2019) 20295, https://doi.org/10.1038/s41598-019-56410-1.
[32] D. Martinez Molina, R. Jafari, M. Ignatushchenko, T. Seki, E.A. Larsson, C. Dan, L. Sreekumar, Y. Cao, P. Nordlund, Monitoring drug target engagement in cells and tissues using the cellular thermal shift assay, Science 341 (2013) 84–87, https://doi.org/10.1126/science.1233606.
[33] F.B.M. Reinhard, D. Eberhard, T. Werner, H. Franken, D. Childs, C. Doce, M. F. Savitski, W. Huber, M. Bantscheff, M.M. Savitski, G. Drewes, Thermal proteome profiling monitors ligand interactions with cellular membrane proteins, Nat. Methods 12 (2015) 1129–1131, https://doi.org/10.1038/nmeth.3652.
[34] I. Becher, T. Werner, C. Doce, E.A. Zaal, I. Tögel, C.A. Khan, A. Rueger, M. Muelbaier, E. Salzer, C.R. Berkers, P.F. Fitzpatrick, M. Bantscheff, M. M. Savitski, Thermal profiling reveals phenylalanine hydroxylase as an off-target of panobinostat, Nat. Chem. Biol. 12 (2016) 908–910, https://doi.org/10.1038/nchembio.2185.
[35] D. Martinez Molina, P. Nordlund, The cellular thermal shift assay: a novel biophysical assay for in situ drug target engagement and mechanistic biomarker studies, Annu. Rev. Pharmacol. Toxicol. 56 (2016) 141–161, https://doi.org/10.1146/annurev-pharmtox-010715-103715.
[36] R. Marullo, E. Werner, H. Zhang, G.Z. Chen, D.M. Shin, P.W. Doetsch, HPV16 E6 and E7 proteins induce a chronic oxidative stress response via NOX2 that causes genomic instability and increased susceptibility to DNA damage in head and neck cancer cells, Carcinogenesis 36 (2015) 1397–1406, https://doi.org/10.1093/carcin/bgv126.
[37] D. Senft, Z.A. Ronai, UPR, autophagy, and mitochondria crosstalk underlies the ER stress response, Trends Biochem. Sci. 40 (2015) 141–148, https://doi.org/10.1016/j.tibs.2015.01.002.
[38] M. Los, M. Mozoluk, D. Ferrari, A. Stepczynska, C. Stroh, A. Renz, Z. Herceg, Z.-Q. Wang, K. Schulze-Osthoff, Activation and caspase-mediated inhibition of PARP: a molecular switch between fibroblast necrosis and apoptosis in death receptor signaling, Mol. Biol. Cell 13 (2002) 978–988, https://doi.org/10.1091/mbc.01-05-0272.
[39] M. Scheffner, J.M. Huibregtse, R.D. Vierstra, P.M. Howley, The HPV-16 E6 and E6-AP complex functions as a ubiquitin-protein ligase in the ubiquitination of p53, Cell 75 (1993) 495–505, https://doi.org/10.1016/0092-8674(93)90384-3.
[40] E.A. White, R.E. Kramer, M.J.A. Tan, S.D. Hayes, J.W. Harper, P.M. Howley, Comprehensive analysis of host cellular interactions with human papillomavirus E6 proteins identifies new E6 binding partners and reflects viral diversity, J. Virol. 86 (2012) 13174–13186, https://doi.org/10.1128/JVI.02172-12.
[41] L. Wang, P. Zhang, D.P. Molkentine, C. Chen, J.M. Molkentine, H. Piao, U. Raju, J. Zhang, D.R. Valdecanas, R.C. Tailor, H.D. Thames, T.A. Buchholz, J. Chen, L. Ma, K.A. Mason, K.-K. Ang, R.E. Meyn, H.D. Skinner, TRIP12 as a mediator of human papillomavirus/p16-related radiation enhancement effects, Oncogene 36 (2017) 820–828, https://doi.org/10.1038/onc.2016.250.
[42] D.P. Molkentine, J.M. Molkentine, K.A. Bridges, D.R. Valdecanas, A. Dhawan, R. Bahri, A.J. Hefner, M. Kumar, L. Yang, M. Abdelhakiem, P.M. Pifer, V. Sandulache, A. Sheth, B.M. Beadle, H.D. Thames, K.A. Mason, C.R. Pickering, R. E. Meyn, H.D. Skinner, p16 represses DNA damage repair via a novel ubiquitin-dependent signaling Cascade, Cancer Res. 82 (2022) 916–928, https://doi.org/10.1158/0008-5472.CAN-21-2101.
[43] S. Bellanger, C.L. Tan, W. Nei, P.P. He, F. Thierry, The human papillomavirus type 18 E2 protein is a cell cycle-dependent target of the SCFSkp2 ubiquitin ligase, J. Virol. 84 (2010) 437–444, https://doi.org/10.1128/jvi.01162-09.
[44] B.A. Bernard, C. Bailly, M.-C. Lenoir, M. Darmon, F. Thierry, M. Yaniv, The human papillomavirus type 18 (HPV18) E2 gene product is a repressor of the HPV18 regulatory region in human keratinocytes, J. Virol. 63 (1989) 4317–4324, https://doi.org/10.1128/jvi.63.10.4317-4324.1989.
[45] A. Chaiwongkot, S. Vinokurova, C. Pientong, T. Ekalaksananan, B. Kongyingyoes, P. Kleebkaow, B. Chumworathayi, N. Patarapadungkit, M. Reuschenbach, M. von Knebel Doeberitz, Differential methylation of E2 binding sites in episomal and integrated HPV 16 genomes in preinvasive and invasive cervical lesions, Int. J. Cancer 132 (2013) 2087–2094, https://doi.org/10.1002/ijc.27906.
[46] S. Bellanger, S. Blachon, F. Mechali, C. Bonne-Andrea, F. Thierry, High-risk but not Low-risk HPV E2 proteins bind to the APC activators Cdh1 and Cdc20 and cause genomic instability, Cell Cycle 4 (2005) 1608–1615, https://doi.org/10.4161/cc.4.11.2123.
[47] D. Patel, D.J. McCance, Compromised spindle assembly checkpoint due to altered expression of Ubch10 and Cdc20 in human papillomavirus type 16 E6- and E7-expressing keratinocytes, J. Virol. 84 (2010) 10956–10964, https://doi.org/10.1128/jvi.00259-10.
[48] M. Scheffner, B.A. Werness, J.M. Huibregtse, A.J. Levine, P.M. Howley, The E6 oncoprotein encoded by human papillomavirus types 16 and 18 promotes the degradation of p53, Cell 63 (1990) 1129–1136, https://doi.org/10.1016/0092-8674(90)90409-8.
[49] J. Hatterschide, A.E. Bohidar, M. Grace, T.J. Nulton, H.W. Kim, B. Windle, I. M. Morgan, K. Munger, E.A. White, PTPN14 degradation by high-risk human papillomavirus E7 limits keratinocyte differentiation and contributes to HPV-mediated oncogenesis, Proc. Natl. Acad. Sci. 116 (2019) 7033–7042, https://doi.org/10.1073/pnas.1819534116.
[50] J. Lim, H. Lilie, H. Kalbacher, N. Roos, D.I. Frecot, M. Feige, M. Conrady, T. Votteler, A. Cousido-Siah, G.C. Bartoli, T. Iftner, G. Trave, C. Simon, Evidence for direct interaction between the oncogenic proteins E6 and E7 of high-risk human papillomavirus (HPV), J. Biol. Chem. 299 (2023), https://doi.org/10.1016/j.jbc.2023.104954.
[51] L. Lignitto, A. Carlucci, M. Sepe, E. Stefan, O. Cuomo, R. Nisticò, A. Scorziello, C. Savoia, C. Garbi, L. Annunziato, A. Feliciello, Control of PKA stability and signalling by the RING ligase praja2, Nat. Cell Biol. 13 (2011) 412–422, https://doi.org/10.1038/ncb2209.
[52] Z. Chen, C. Peng, C. Jin, Y. Wang, T. Wang, P. Yang, W. Peng, Q. Sun, H. Xu, H. Nie, X. Wang, J. Tang, Y. Sun, Y. Feng, PJA2 suppresses colorectal cancer progression by controlling HDAC2 degradation and stability, Adv. Sci. (2025), https://doi.org/10.1002/advs.202401964, 2401964.
[53] M. Grønbæk-Thygesen, C. Kampmeyer, K. Hofmann, R. Hartmann-Petersen, The moonlighting of RAD23 in DNA repair and protein degradation, Biochim. Biophys. Acta, Gene Regul. Mech. 2023 (1866) 194925, https://doi.org/10.1016/j.bbagrm.2023.194925.
[54] L. Hui, S. Zhang, M. Wudu, H. Ren, Y. Xu, Q. Zhang, X. Qiu, CBLL1 is highly expressed in non-small cell lung cancer and promotes cell proliferation and invasion, Thorac. Cancer 10 (2019) 1479–1488, https://doi.org/10.1111/1759-7714.13097.
[55] J.-J. Escuder-Rodríguez, A. Rodríguez-Alonso, L. Jove, M. Quiroga, G. Alfonsín, A. Figueroa, Beyond destruction: emerging roles of the E3 ubiquitin ligase Hakai, Cell. Mol. Biol. Lett. 30 (2025) 9, https://doi.org/10.1186/s11658-025-00693-y.
[56] X. Guo, Y. Li, B. Wan, Y. Lv, X. Wang, G. Liu, P. Wang, TRIM26 Inhibits Gastric Cancer Development by Regulating SLC7A11-mediated Ferroptosis Pathwa, 2022, https://doi.org/10.21203/rs.3.rs-1473856/v1.
[57] N. Huang, X. Sun, P. Li, X. Liu, X. Zhang, Q. Chen, H. Xin, TRIM family contribute to tumorigenesis, cancer development, and drug resistance, Exp. Hematol. Oncol. 11 (2022) 75, https://doi.org/10.1186/s40164-022-00322-w.
[58] Y. Sun, P. Lin, X. Zhou, Y. Ren, Y. He, J. Liang, Z. Zhu, X. Xu, X. Mao, TRIM26 promotes non-small cell lung cancer survival by inducing PBX1 degradation, Int. J. Biol. Sci. 19 (2023) 2803–2816, https://doi.org/10.7150/ijbs.81726.
[59] D. Zheng, J. Ning, H. Deng, Y. Ruan, F. Cheng, TRIM26 inhibits clear cell renal cell carcinoma progression through destabilizing ETK and thus inactivation of AKT/mTOR signaling, J. Transl. Med. 22 (2024) 481, https://doi.org/10.1186/s12967-024-05273-w.
[60] B. Cooper, S. Schneider, J. Bohl, Y.H. Jiang, A. Beaudet, S. Vande Pol, Requirement of E6AP and the features of human papillomavirus E6 necessary to support degradation of p53, Virology 306 (2003) 87–99, https://doi.org/10.1016/S0042-6822(02)00012-0.
[61] S. Strickland, N. Brimer, C. Lyons, S.B. Vande Pol, Human papillomavirus E6 interaction with cellular PDZ domain proteins modulates YAP nuclear localization, Virology 516 (2018) 127–138, https://doi.org/10.1016/j.virol.2018.01.003.
[62] T. Kiyono, A. Hiraiwa, M. Fujita, Y. Hayashi, T. Akiyama, M. Ishibashi, Binding of high-risk human papillomavirus E6 oncoproteins to the human homologue of the Drosophila discs large tumor suppressor protein, Proc. Natl. Acad. Sci. USA 94 (1997) 11612–11616, https://doi.org/10.1073/pnas.94.21.11612.
[63] T. Ansari, N. Brimer, S.B. Vande Pol, Peptide interactions stabilize and restructure human papillomavirus type 16 E6 to interact with p53, J. Virol. 86 (2012) 11386–11391, https://doi.org/10.1128/JVI.01236-12.
[64] E.A. White, K. Münger, P.M. Howley, High-risk human papillomavirus E7 proteins target PTPN14 for degradation, mBio 7 (2016) e01530–16, https://doi.org/10.1128/mBio.01530-16.
[65] M. Brunet, C. Vargas, D. Larrieu, J. Torrisani, M. Dufresne, E3 ubiquitin ligase TRIP12: regulation, structure, and physiopathological functions, Int. J. Mol. Sci. 21 (2020) 8515, https://doi.org/10.3390/ijms21228515.
[66] C. Xia, C. Xiao, H.Y. Luk, P.K.S. Chan, S.S. Boon, The ubiquitin specific protease 7 stabilizes HPV16E7 to promote HPV-mediated carcinogenesis, Cell. Mol. Life Sci. 80 (2023) 278, https://doi.org/10.1007/s00018-023-04941-2.
[67] Y. Perez-Riverol, C. Bandla, D.J. Kundu, S. Kamatchinathan, J. Bai, S. Hewapathirana, N.S. John, A. Prakash, M. Walzer, S. Wang, J.A. Vizcaíno, The PRIDE database at 20 years: 2025 update, Nucleic Acids Res. 53 (2025) D543–D553, https://doi.org/10.1093/nar/gkae1011.